INORGANIC CHEMISTRY FRONTIERS

RESEARCH ARTICLE

View Article Online
View Journal

Cite this: DOI: 10.1039/d5qi01181g

Aqueously synthesized and reusable Ce(IV)-based metal–organic frameworks with aliphatic multicarboxylate linkers for highly efficient Pb^{2+} removal from water

Nikolaos E. Anastasiadis,†[a] Vasiliki I. Karagianni,†[a] Pantelis Kotidis,[b] Christos Dimitriou,[c] Ioannis Vamvasakis,[d] Theodore Lazarides,[e] Giannis S. Papaefstathiou,[b] Yiannis Deligiannakis,[c] Gerasimos S. Armatas,[d] Emilia Buchsteiner[f] and Manolis J. Manos *[a]

New Ce(IV) metal–organic frameworks (MOFs) are reported based on the aliphatic linker butane-1,2,3,4-tetracarboxylic acid (H_4BTCA). These materials were prepared using an eco-friendly aqueous-based synthesis, and their structures were elucidated through microcrystal electron diffraction (MicroED) and powder X-ray diffraction (PXRD). They feature an 8-coordinated net with a **bcu** topology, rarely observed for Ce(IV) MOFs. Interconversion between the MOFs was easily achieved *via* treatment with basic or formic acid solutions, revealing the breathing of the MOFs' frameworks. The MOFs were investigated for their ability to sorb Pb^{2+} under both batch and continuous flow conditions. The results showed relatively high Pb^{2+} sorption capacities (up to 254 mg Pb per g) and an exceptional capability for the rapid removal (in less than 10 min of MOF–solution contact) of Pb^{2+} from low initial concentrations of complex solutions and real-world water samples. Notably, the materials in the form of calcium alginate-based beads used as a stationary phase in a column (along with sea sand) demonstrate a remarkable ability to capture Pb^{2+} under continuous flow, showing decent removal capacities, excellent regeneration efficiency, and reusability. The mechanism of the Pb^{2+} sorption process was determined *via* experimental data, indicating strong interactions of the MOF's functional groups (carboxylate and hydroxide groups) with the Pb^{2+} ions.

Received 21st May 2025,
Accepted 14th August 2025

DOI: 10.1039/d5qi01181g

rsc.li/frontiers-inorganic

1. Introduction

MOFs have been at the forefront of materials science for the last 15–20 years. This is due to their exceptional structural diversity and extraordinary properties related to various fields and applications.[1–7] MOFs, among other applications, exhibit significant promise in water remediation due to their unique combination of a porous structure, diverse functional groups, and remarkable stability in aqueous media.[8–11] Most MOF sorbents are based on aromatic ligands bearing various functional groups. Examples include the Zr^{4+} MOFs with terephthalate ligands or polyaromatic tetracarboxylic acids, Al-MOFs with the MIL-53 structure type, ZIFs, ionic MOFs, *etc.*[11–14] These materials have shown exceptional sorption capacities for various toxic species, including heavy metal cations, oxoanions, organic dyes, *etc.* Although such materials appear attractive for practical applications, the synthesis of most of them requires the use of organic solvents (*e.g.*, DMF), which are costly and sometimes highly toxic.

Aromatic ligands have poor solubility in water, with some exceptions,[15,16] so MOFs with such ligands can be isolated primarily *via* non-aqueous synthesis. Alternatively, MOFs with aliphatic polycarboxylic linkers (aliphatic linker-MOFs, **AL-MOFs**) have recently attracted the attention of researchers.[17] As aliphatic polycarboxylic ligands are soluble in water (at room temperature or 80–100 °C), **AL-MOFs** can be isolated *via* aqueous-based synthesis. In addition, **AL-MOFs** can be prepared within a few hours or minutes. Furthermore, the cost of most aliphatic polycarboxylic ligands is much less compared to that of aromatic polycarboxylic acids. Additionally, commercially available aliphatic polycarboxylic ligands with various

[a]Department of Chemistry, University of Ioannina, GR-45110 Ioannina, Greece. E-mail: emanos@uoi.gr
[b]Department of Chemistry, National and Kapodistrian University of Athens, 15771 Athens, Greece
[c]Department of Physics, University of Ioannina, 45110 Ioannina, Greece
[d]Department of Materials Science and Engineering, University of Crete, 70013 Heraklion, Greece
[e]Department of Chemistry, Aristotle University of Thessaloniki, 54124 Thessaloniki, Greece
[f]Rigaku Europe SE, Hugenottenallee 167, 63263 Neu-Isenburg, Germany
†These authors contributed equally to this work.

functional groups (–SH, NH_2, COOH, *etc*.) can be used to build MOFs with high sorption efficiency for multiple species.[18–20] Thus, **AL-MOFs** could be highly promising sorbents for toxic species and attractive for large-scale preparation and, consequently, for actual applications in wastewater treatment. Nevertheless, limited studies have been conducted on MOFs from this family for the sorption of toxic ions and other species from aqueous media. Specifically, there are few reports on the sorption of Hg^{2+}, Ba^{2+}, oxoanions, organophosphates, precious metal ions, and nanoparticles by Zr^{4+} MOFs with aliphatic dicarboxylic ligands bearing –SH, $–SO_3H$, and NH_3^+-surface functional groups.[18,19,21–23] In contrast, no ion sorption studies have been reported for Ce(IV)-based **AL-MOFs**,[24–27] which share similar structural features with the corresponding Zr(IV) materials.

Herein, we report new Ce(IV) MOFs based on the inexpensive ligand butane-1,2,3,4-tetracarboxylic acid (H_4BTCA), specifically $[Ce_6O_4(OH)_{5.4}(H_2BTCA)_4(HCOO)_{2.6}(H_2O)_{1.4}]$·solvent (**AL-MOF-1**), $[Ce_6O_4(OH)_8(H_2BTCA)_4(H_2O)_6]$·solvent (**AL-MOF-2**) and the semi-amorphous **AL-MOF-3** exhibiting a similar composition to **AL-MOF-2**. The newly synthesized MOFs can be isolated in high yield and on a relatively large scale (up to 7.5 g) *via* aqueous-based synthesis within a few minutes (25–30 min). The MOFs feature an 8-coordinated **bcu** net, seldom seen for Ce(IV) MOFs, and several non-coordinated COOH-functional groups, a characteristic not present in reported Ce^{IV} MOFs. The presence of free COOH in the structure of the MOFs, along with terminal OH ligands, gives them exceptional sorption capabilities for heavy metal ions, such as Pb^{2+}. They show rapid sorption kinetics, high sorption capacity (up to 254 mg Pb per g), and efficiency for removing Pb^{2+} ions in the presence of competitive (non-toxic) ions. Furthermore, the MOFs in their composites with calcium alginate (CA) can remove Pb^{2+} under flow conditions using a column filled with the MOF-CA composite. The MOF-CA-based column can be regenerated and reused for Pb^{2+} sorption under continuous flow for several runs. Overall, the **AL-MOF-1–3** materials represent particularly attractive sorbents for heavy metal ions. They possess an exceptional sorption capacity and can be prepared *via* rapid, eco-friendly synthetic methods with high yield and scalability.

2. Results and discussion

2.1 Synthesis and characterization

AL-MOF-1 was synthesized from a reaction mixture of ceric ammonium nitrate (CAN), water, and formic acid (HFA) *via* thermal treatment at 80 °C under magnetic stirring, which resulted in the isolation of the MOF with high yield and purity. Significantly, the synthesis of **AL-MOF-1** could be easily scaled up, yielding at least 7.5 g of the MOF within 25–30 minutes. Considering the reagents' bulk prices, the MOF synthesis cost is estimated at ~8 € per kg. The space–time yield for the green synthesis of **AL-MOF-1** is calculated to be 1800 kg m^{-3} day^{-1}, which compares well with industrial preparations of MOFs.[28–30] Unfortunately, obtaining single crystals of the MOF was impossible. **AL-MOF-1** is received as microcrystalline powder based on particle aggregates of <3 μm (Fig. 1A). Nevertheless, we were able to determine and refine the structure of **AL-MOF-1** using microcrystal electron diffraction (MicroED, Fig. S1). Although the determined and refined structure is highly disordered, the overall structural model and connectivity can still be correctly identified (Fig. 1B). **AL-MOF-1** crystallizes in the tetragonal space group *I*4/*mmm* with a = 13.22(16) Å, c = 19.4(4) Å and V = 3391(108) $Å^3$. It is based on Ce_6 secondary building units (SBUs), featuring bridging oxo and hydroxy ligands, as well as mixed bridging formate/terminal water-hydroxide groups (see below). Each cluster is connected *via* the 1,2-COO^- groups of the H_2BTCA^{2-} ligands, with eight adjacent clusters, forming an 8-c net with a **bcu** topology. We should note that this is only the second example of a MOF with Ce_6 units showing such structural topology.[27] Most reported MOFs based on Ce_6 SBUs exhibit an **fcu** net,[31,32] whereas a few examples show **hex**, **spn**, **ftw**, **scu**, **csq**, **bct** and **reo** topologies.[24,26,27,33–37] The ligation of H_2BTCA^{2-} to Ce ions through the 1,2-COO^- groups leaves two uncoordinated COOH units per ligand, which could not be identified due to the limited diffraction quality and the high disorder of the organic linkers. Interestingly, despite the poor diffraction quality and the limitation of the ED method, guest water and highly disordered formic acid molecules could be located in the material's pores (Fig. S2). As several atoms in the structure of **AL-MOF-1** are positionally disordered due to the space group symmetry constraints, and the H_2BTCA ligand could not be correctly identified, it is challenging to determine the correct pore sizes of the MOF. Thus, we decided to transform the *I*4/*mmm* space group of the structure determined from MicroED data into the lower symmetry $I\bar{4}$ space group, aiming to obtain a structural model of the MOF with no positional disorder (Fig. 1C). Rietveld refinement using PXRD data and TOPAS[38] software yielded reasonably good results (Fig. S3). The refined structure based on PXRD data is similar to that obtained from MicroED data; however, the lower-symmetry space group of the PXRD structural model resolves any positional disorder, allowing a relatively reliable identification of the H_2BTCA^{2-} linkers. Utilizing this structural model, the pore sizes can be estimated. Consequently, the pore sizes of **AL-MOF-1** are 1.9–4.7 Å, as determined from the pore analysis utility of mercury.[39] The limited pore size is rationalized by the orientation of uncoordinated COOH groups towards the interior of the MOF's structure. The porosity of **AL-MOF-1** was investigated using N_2 adsorption measurements, which indicated a BET surface area of only 16 m^2 g^{-1} (Fig. S4). We also attempted to further characterize the porosity of **AL-MOF-1** by performing CO_2 adsorption measurements. However, even at 273 K, the CO_2 uptake was very low, reflecting the limited overall porosity (Fig. S5). To verify the presence of the organic linkers in the MOF, ^1H NMR data for the MOF digested in D_2O/NaOH were recorded (Fig. S6 and S7). Before the ^1H NMR studies, the MOF was pre-heated to 149 °C inside a thermogravimetric analyzer (TGA) to directly relate the results from

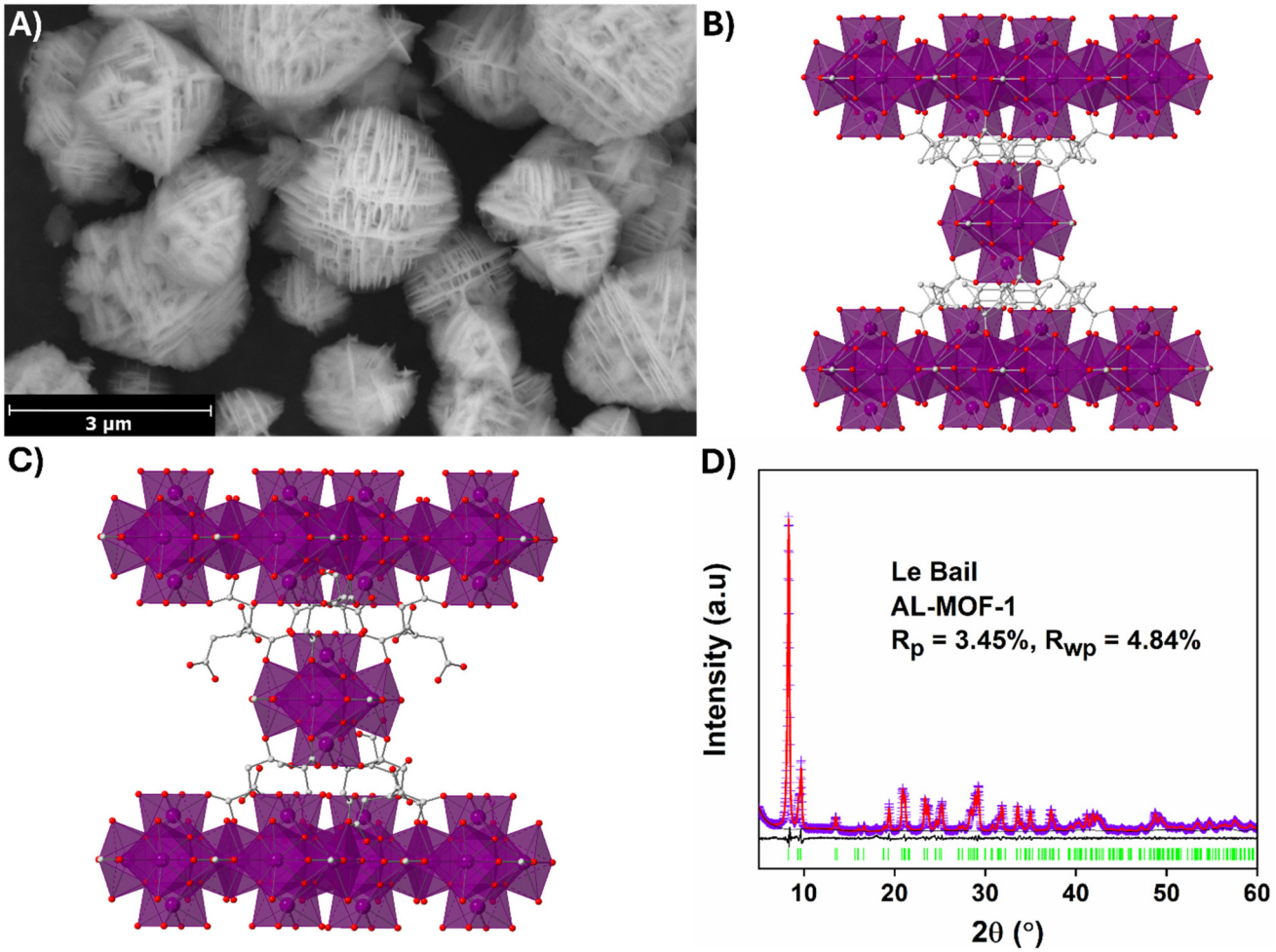

Fig. 1 (A) FE-SEM image of **AL-MOF-1**, (B) structural model of **AL-MOF-1** by MicroED analysis, (C) structural model of **AL-MOF-1** by Rietveld refinement, and (D) Le Bail plot of **AL-MOF-1**. Violet crosses: experimental points; red line: calculated pattern; black line: difference pattern (exp. – calc.); and green bars: Bragg positions. Refined unit cell parameters: a = 12.99(2) Å, c = 18.89(4) Å, V (Å^3) = 3187(2), and space group: $I4/mmm$.

^{1}H NMR with those from TGA. ^{1}H NMR revealed a ratio of BTCA : formate = 4 : 2.6. Considering a partial occupancy for the formate ions, terminal water and hydroxide ligands should be present to complete the coordination sphere of the Ce ions. The composition for **AL-MOF-1** can be calculated from the general formula $Ce_6O_4(OH)_{4+2x-y}(H_2BTCA)_{6-x}(HCOO)_y(H_2O)_{2x-y}$, considering that OH/$H_2O$ terminal ligands replace each missing linker not filled by the modulator.[40] Thus, replacing x = 2 (as found from MicroED data) and y = 2.6 (as seen from ^{1}H NMR data) in the above formula, the formula of **AL-MOF-1** is $[Ce_6O_4(OH)_{5.4}(H_2BTCA)_4(HCOO)_{2.6}(H_2O)_{1.4}]$. This composition was further verified using TGA data (Fig. S8). Ce 3d XPS spectra of **AL-MOF-1** were also recorded (Fig. S9). The presence of multiple overlapping peaks and the potential reduction of Ce(IV) to Ce(III) upon exposure to X-ray radiation preclude a reliable estimation of Ce oxidation states.[41] Thus, a simple method was employed to identify the Ce oxidation state. The room-temperature magnetic susceptibility of AL-MOF-1 was negative, revealing the diamagnetic nature of the material and the exclusive presence of Ce(IV) with no detectable Ce(III) contribution (Fig. S10). In addition, the purity and crystallinity of the MOF were confirmed from PXRD and Le Bail analysis using TOPAS[38] (Fig. 1D).

Aiming to remove excess acid and deprotonate the free carboxylic acids, we treated the MOF with 0.1 M NaOH solution (with the final pH of MOF's suspensions adjusted to 7.5). Surprisingly, the PXRD pattern of the resulting material, **AL-MOF-2**, showed a significant shift towards higher angles related to **AL-MOF-1** (Fig. 2A). This revealed a contraction of the unit cell of the MOF upon treatment with the alkaline solution (Fig. S11). ^{1}H NMR on the MOF digested in basic solution indicated a negligible amount of formate ligands (Fig. S12). MicroED studies were also performed to gain insight into the crystal structure of **AL-MOF-2** (Fig. S13). These studies confirmed the contracted unit cell of the MOF with a unit cell volume ~9% smaller than that of **AL-MOF-1** (Fig. 2B). A contraction of ~0.8 Å is observed along the a and b axes, attributed to the replacement of the bridging formate ligands by terminal water/hydroxide ligands. All Ce ions in **AL-MOF-1** are eight-coordinated in a square-antiprismatic geometry; however, in **AL-MOF-2**, four of the six Ce ions adopt a similar

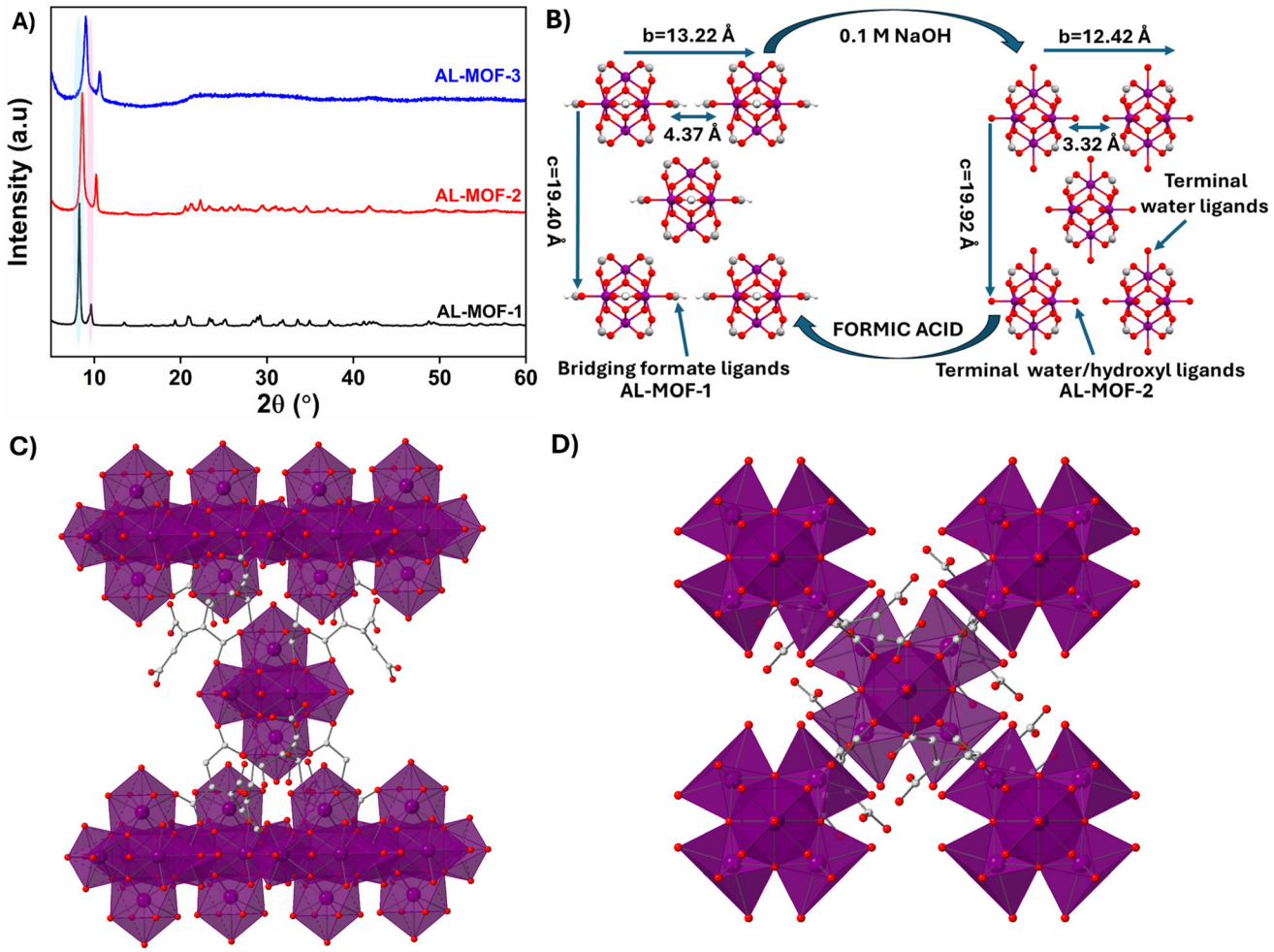

Fig. 2 (A) PXRD patterns of **AL-MOF-1**, **AL-MOF-2** and **AL-MOF-3**. (B) Schematic illustration of the reversible structural transformation: **AL-MOF-1** is converted into **AL-MOF-2** upon treatment with NaOH, while **AL-MOF-2** reverts to **AL-MOF-1** upon exposure to formic acid. Structural model of **AL-MOF-2** by Rietveld refinement viewed down the (C) *b*-axis and (D) *c*-axis.

coordination geometry. The remaining Ce ions are nine-coordinated in mono-capped square-antiprismatic geometry bearing an additional water terminal ligand.[24,42] Considering the replacement of formate ligands by water/hydroxide groups in the coordination environment of 4 Ce ions and the insertion of additional water terminal ligands in the rest of the Ce centers, the formula of **AL-MOF-2** can be written as $[Ce_6O_4(OH)_8(H_2BTCA)_4(H_2O)_6]$. Similarly to **AL-MOF-1**, a model of **AL-MOF-2** in the $I\bar{4}$ space group was built to determine the pore sizes. Rietveld analysis was then performed, providing reasonably good results (Fig. S14). Based on the refined structure (Fig. 2C and D), the pore sizes of **AL-MOF-2** were determined to be 1.2–4.0 Å, which are 15–37% smaller than those for **AL-MOF-1**. This further confirms the contraction of the MOF structure upon the removal of the formate ligands. SEM images indicated similar morphology and sizes for the **AL-MOF-2** particles compared to those of **AL-MOF-1** (Fig. S15). In addition, **AL-MOF-2** exhibits a negligible BET surface area (4 m^2 g^{-1}) (Fig. S16) and limited CO_2 adsorption (Fig. S5). Interestingly, when formic acid is applied to **AL-MOF-2**, **AL-MOF-1** is regenerated, as formate is reconnected with the Ce(IV) centers (Fig. S17). In contrast, no change in the structure of **AL-MOF-2** was observed when it was treated with bulkier aliphatic carboxylic acids (such as acetic and 2-mercaptosuccinic acid) other than formic acid (Fig. S18). The increased size of the former and their significant steric interactions with the side groups of the H_2BTCA^{2-} ligands may prohibit their entrance into the MOF's framework. The negative magnetic susceptibility of **AL-MOF-2** suggests the exclusive presence of Ce(IV), with no evidence of paramagnetic Ce(III) species.

To achieve more effective deprotonation of the material, **AL-MOF-1** was treated with 1 M NaOH (with the final pH adjusted to 9.5). This resulted in a new material (**AL-MOF-3**) with diminished crystallinity (Fig. 2A), having a similar chemical composition to that of **AL-MOF-2**, as confirmed by ^{1}H NMR data (Fig. S20), indicating a negligible amount of formate. Unfortunately, due to diminished crystallinity, the structural determination of **AL-MOF-3** was not possible. Interestingly, the

nearly amorphous **AL-MOF-3** can be converted into the crystalline **AL-MOF-1** by treating the first material with formic acid (Fig. S21). Still, no structural modification occurs when **AL-MOF-3** is treated with bulkier aliphatic acids (Fig. S22). **AL-MOF-3** is also a non-porous material with a BET surface area of 6 $m^2\ g^{-1}$ (Fig. S23) and low CO_2 uptake (Fig. S5). The observed diamagnetic behavior, indicated by the negative magnetic susceptibility of the material, further corroborates that **AL-MOF-3** is composed excessively of Ce(IV).

The IR spectra of the three materials are similar (Fig. S24). However, the absorption peak assigned to the free COOH group is somewhat weaker in the IR spectra of **AL-MOF-2** and **AL-MOF-3** than in the spectrum of **AL-MOF-1**. This is consistent with the partial deprotonation of the free carboxylic acid groups in **AL-MOF-2** and **AL-MOF-3** materials. EDS analysis reveals the presence of Na in treated **AL-MOF-2** and **AL-MOF-3** samples (Fig. S15 and S19), which also indicates the deprotonation of the carboxylic acid groups. We should, however, mention that Na^+ ions are likely located on the surface of **AL-MOF-2** and **3** materials, considering the relatively large size of hydrated Na^+ ions (~4.4 Å) compared to the tiny pores of the MOFs.

Concerning the stability of **AL-MOF-1** *vs.* pH, we observed that the material retains its structure from pH 0 to 6, whereas from pH 7 and above, **AL-MOF-1** is gradually transformed into **AL-MOF-2** and **3** (Fig. S25 and S27). Also, the stability studies of **AL-MOF-1** in different solvents, such as DMF, DMSO, and MeOH, indicated that the structural characteristics of the material remain intact upon treatment with organic solvents (Fig. S26).

2.2 Heavy metal ion sorption properties

2.2.1 Batch sorption studies. The presence of several uncoordinated COOH and terminal hydroxide groups in **AL-MOF-1**, **AL-MOF-2**, and **AL-MOF-3**, which are excellent ligands for binding metal ions,[43,44] motivated us to study the sorption properties of the MOF for heavy metal ions. We focused on removing Pb^{2+}, as it is one of the most toxic heavy metal ions frequently found in contaminated water resources and wastewater.[45–47] Pristine **AL-MOF-1** has a positive surface charge (zeta potential ~8 mV, at pH = 7) (Fig. S28). Before the sorption studies, **AL-MOF-1** was treated with a mild alkaline solution to remove unreacted acids (formic or H_4BTCA) and induce an anionic surface charge, which is beneficial for the sorption of cations. Indeed, the zeta potential of the activated MOF was found to be −19.8 mV at pH = 7 (Fig. S29). Besides the zeta potential values, there is no differentiation in the structural characteristics of pristine and activated **AL-MOF-1** (Fig. S30). Our investigations started with the determination of sorption kinetics. We have performed two sets of kinetic sorption tests, one involving a low initial Pb^{2+} concentration (1 ppm) and a second with a much higher Pb^{2+} concentration (100 ppm). The sorption with the low initial Pb^{2+} concentration is rapid, as the Pb^{2+} concentration was determined to be 25 ppb after only 30 seconds of solution treatment with the MOF (Fig. 3A). Notably, the concentration of Pb^{2+} was found to be well below (3.2 ppb) the acceptable limit (10 ppb) of Pb^{2+} in drinking water within 10 min of contact of the solution with the MOF sorbent. As the sorption rate is relatively fast, fitting the data to known kinetic models was not possible. The sorption tests with a high initial Pb^{2+} concentration indicate that the sorption process is relatively slow compared to that with low initial Pb^{2+} concentration, achieving ~73% removal after 48 h treatment of the Pb^{2+} solution with the MOF (Fig. S31). Unfortunately, no reliable fitting of the sorption kinetics data could be achieved. These results show that the sorption rate is relatively fast at low Pb^{2+} levels but slower at high concentrations. This is likely related to the sorption mechanism involving electrostatic Pb^{2+}–MOF interactions at low Pb^{2+} concentrations at the surface of MOF particles, whereas capturing additional Pb^{2+} amounts requires the formation of coordination bonds between Pb^{2+} and COOH or OH groups, which is a relatively slow process. More details about the Pb^{2+} sorption mechanism are given below. As a second step of our investigations, we performed sorption isotherm studies (at pH ~5) using 48 hour treatment times. The data were fitted with the

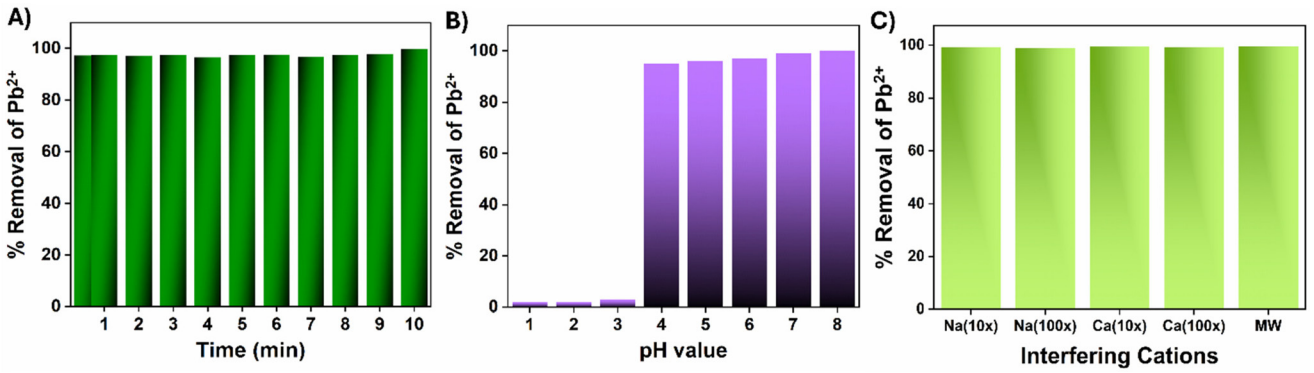

Fig. 3 (A) Kinetics of Pb^{2+} sorption for activated **AL-MOF-1** (initial Pb concentration = 1 ppm, pH ~7), (B) Pb^{2+} sorption data for activated **AL-MOF-1** at variable pH values (1–8) (initial Pb concentration = 1 ppm) and (C) Pb^{2+} sorption data for activated **AL-MOF-1** in the coexistence of various cations (100-fold excess) and for an artificially contaminated bottled water sample (initial Pb concentration = 1 ppm, pH ~7). Composition of mineral water (MW): Ca^{2+} = 101 ppm, Mg^{2+} = 1.54 ppm, Na^+ = 3.11 ppm, K^+ = 0.62 ppm, pH = 7.5.

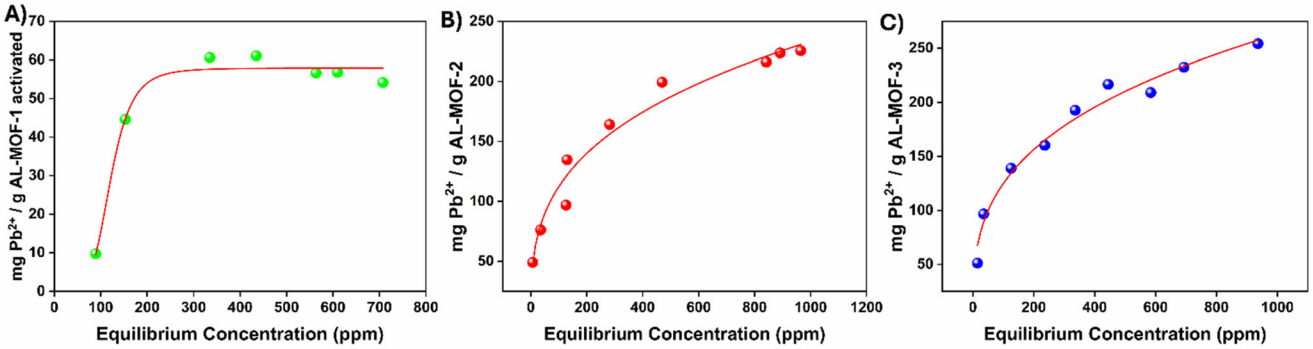

Fig. 4 Isotherm Pb^{2+} sorption data for (A) activated **AL-MOF-1**; the red line signifies the data fitted with the Langmuir–Freundlich model (R^2 = 0.97, q_e = 58.0 ± 1.0 mg g^{-1}, b = 0.007 ± 0.001 L mg^{-1} and n = 0.19 ± 0.03 (contact time, t = 48 h)), (B) **AL-MOF-2**; the red line signifies the data fitted with the Freundlich model (R^2 = 0.97, K_F = 26.0 ± 11.0 and n = 3.15 ± 0.3 (contact time, t = 48 h)), and (C) **AL-MOF-3**; the red line signifies the data fitted with the Freundlich model (R^2 = 0.97, K_F = 28.2 ± 4.3 and n = 3.05 ± 0.2 (contact time, t = 48 h)).

Langmuir–Freundlich model[48] (eqn (S1)), consistent with monolayer and multilayer sorption mechanisms (Fig. 4A). The maximum sorption capacity determined from the sorption isotherm data was 58.0 ± 1.0 mg Pb per g of the MOF.

In addition, we determined the effect of pH on the sorption of Pb^{2+} by the MOF. These experiments were conducted with a low initial Pb^{2+} concentration (1 ppm) to prevent the precipitation of lead hydroxide that occurs for high Pb^{2+} concentrations at neutral to alkaline solutions (Fig. 3B). The results indicate that almost quantitative Pb^{2+} removal (95%) is achieved in solutions with pH > 4, whereas sorption is diminished in a highly acidic environment (pH ≤ 3). The zeta potential of the MOF is still negative at pH~3, thus excluding repulsive interactions between MOF and Pb^{2+}. Therefore, the decreased performance of the material under these conditions is attributed to the high excess of H^+ (~200-fold) relative to the Pb^{2+} concentration, resulting in intense competition by H^+ for Pb^{2+} sorption.

Furthermore, we investigated the effect of competitive ions on the sorption of Pb^{2+} by the MOF. Specifically, the Pb^{2+} sorption capacity of the MOF was studied in the presence of 10- and 100-fold excess Na^+ and Ca^{2+} cations, which are present in relatively high concentrations in aqueous media. The Pb^{2+} sorption is not affected by the presence of the competitive ionic species, as Pb^{2+} % removal was found to be >98% in all sorption tests (Fig. 3C). Furthermore, we have tested the Pb^{2+} sorption performance of the MOF in natural spring water spiked with one ppm of Pb^{2+}. This solution contained several cations (Ca^{2+}, Mg^{2+}, Na^+, K^+, and NH_4^+) in excess up to 100-fold compared to Pb^{2+}, respectively. Still, the MOF shows a Pb^{2+} removal of 99.5% despite a significant excess of several competitive species.

AL-MOF-2 and **AL-MOF-3** were also investigated for Pb^{2+} sorption (Fig. S32 and S33). These materials exhibited enhanced sorption capabilities compared to **AL-MOF-1**, with maximum sorption capacities of 233.0 and 254.0 mg Pb^{2+} per g for **AL-MOF-2** and **AL-MOF-3**, respectively (Fig. 4B and C). The improved sorption efficiencies of these materials are attributed to (a) their increased number of terminal hydroxide groups being effective ligands for Pb^{2+} and (b) possible deprotonation of some of the free COOH groups, with the resulting COO^- groups strongly binding Pb^{2+} ions. **AL-MOF-2** and **3** also showed the capability for efficiently removing Pb^{2+} in the presence of several interfering species (Fig. S34).

2.2.2 Column sorption studies. Concerning the practical application of the sorbent for water treatment, we have investigated the Pb^{2+} sorption properties of the MOF under continuous flow conditions. **AL-MOF-1** is in the microcrystalline form, so it is unsuitable for use as a stationary phase of the column. Thus, we have transformed the MOF into a composite with calcium alginate, which has a bead-like form (Fig. S35A).[49,50] For these sorption tests, we used a mixture of MOF-CA beads and sea sand to distribute the sorbent over a longer column length, thereby enhancing sorption efficiency by increasing the contact time of the solution with the MOF-CA material (Fig. S35B).[16,51,52] The column sorption experiments were performed with a Pb^{2+} solution of relatively high concentration (80 ppm). The results revealed that Pb^{2+} removal exceeded 60% when 50 mL of the Pb^{2+} solution was passed through the column, whereas the removal percentage remained above 40% even after passing 100 mL of the solution (Fig. 5A). Interestingly, the sorption efficiency was significantly enhanced after the column was treated with 0.1 M HCl to regenerate the sorbent. Specifically, the Pb^{2+} removal percentage for the second run of the column was ~80% for 50 mL of the effluent, *i.e.*, ~1.5 times higher than the removal percentage for the column after the regeneration process. The % Pb^{2+} removal was found to be ~60%, even for the treatment of a 100 mL solution, which is significantly higher than the corresponding value determined in the first run of the column. After regeneration with 0.1 M HCl acid solution, a third run of the column yielded similar or even slightly better results than the second run. A fourth run of the column, after the regeneration process, showed even better results. This unusual column behavior is attributed to the release of formate upon treatment with the acidic solution. Indeed, ^1H NMR studies confirmed a

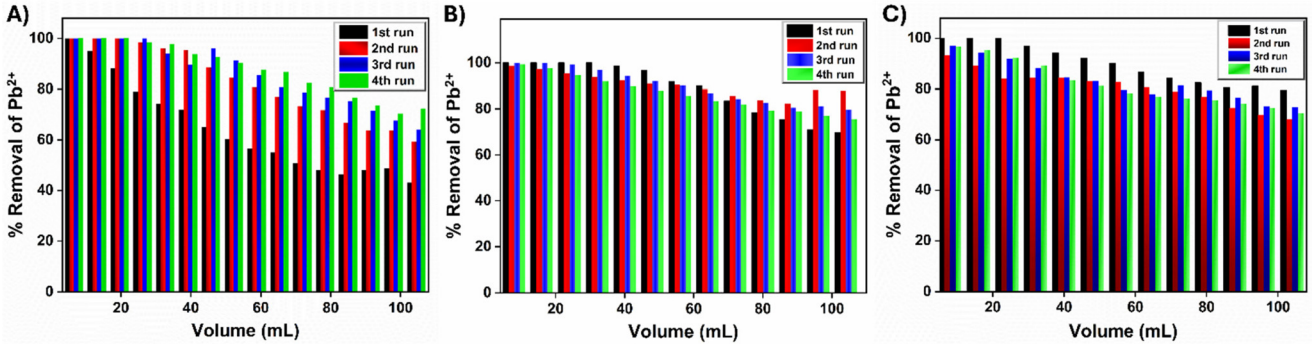

Fig. 5 Column sorption studies of (A) activated **AL-MOF-1**, (B) **AL-MOF-2** and (C) **AL-MOF-3**, $C_{initial}$ = 83 ppm, pH = 5.0, and flow rate = 1.0 mL min^{-1}.

substantial removal of formate ligands upon treatment of **AL-MOF-1** with 0.1 M HCl (Fig. S36). The released formate ligands are replaced by water and/or hydroxide ligands, as evidenced by the MicroED study of **AL-MOF-2**. The hydroxide groups formed after the acid treatment act as additional binding sites for Pb^{2+}, thereby enhancing the sorption efficiency of the column following acid-induced regeneration. This explanation is further supported by the sorption results for **AL-MOF-2** and **AL-MOF-3** materials, which are discussed below. Finally, we performed column sorption experiments with natural spring water intentionally contaminated with Pb^{2+} traces (80 ppb). The results revealed that ~5 L of the Pb^{2+}-spiked natural spring water could be effectively decontaminated after passing through the column, with no detectable Pb remaining. This indicates the material's superior performance for treating genuine water samples (Fig. S37).

Column sorption studies were also conducted for the **AL-MOF-2** and **AL-MOF-3**/calcium alginate composites. Again, the sorption efficiencies were significantly higher than those for the **AL-MOF-1/CA** composite (Fig. 5B and C). Thus, the % Pb^{2+} removal capacities were 70% and 80% after passing 100 mL of Pb^{2+} solution in the first runs of the **AL-MOF-2/CA** and **AL-MOF-3/CA** columns, respectively, *vs.* 50% removal of Pb^{2+} for the same effluent volume in the first run of the **AL-MOF-1/CA** column. The **AL-MOF-2/CA** and **AL-MOF-3/CA** composites can be regenerated and reused with no loss of their capacity, at least for four runs. Also, the PXRD diagram of **AL-MOF-2/CA** beads indicates that the composite retains its crystal structure after the 4^{th} column run (Fig. S38). We should also note that the unusual behavior of the **AL-MOF-1/CA** composite, showing enhanced sorption capacity after acid treatment, is not observed in the **AL-MOF-2/CA** and **AL-MOF-3/CA** composites. Specifically, the sorption efficiencies of the **AL-MOF-2/CA** and **AL-MOF-3/CA** columns are only slightly differentiated among the various runs. Based on the previous discussion, this is anticipated, considering that **AL-MOF-2** and **AL-MOF-3** contain negligible formate ligands. Thus, the acid-based regeneration process does not affect their chemical composition, unlike **AL-MOF-1**, which releases formate ligands upon acid treatment.

2.3 Comparison of AL-MOF-1, 2, 3 with known Pb^{2+} sorbents

Several MOFs and other sorbents have been reported for their Pb^{2+} sorption properties (Table S2), revealing excellent performance with sorption capacities up to 570 mg g^{-1}. However, their synthesis typically involves solvothermal conditions that require elevated temperatures (>100 °C), extended reaction times (from 20 up to 72 h), and the use of toxic and costly organic solvents (Table S3).[48,53–60] Additionally, the organic ligands used in many MOF-based Pb^{2+} sorbents are not always commercially available, which further increases the complexity and cost of MOF production. Reusability also remains a challenge, as many of these materials cannot be regenerated and reused, representing a significant drawback for practical applications in wastewater treatment.[48,53,57] Furthermore, studies with MOFs for Pb^{2+} sorption were mainly focused on batch sorption experiments, with only limited reports presenting sorption data under continuous flow conditions.[53]

In contrast to previously reported MOFs, **AL-MOF-1** exhibits a low Pb^{2+} sorption capacity (58.0 mg g^{-1}). Still, it is synthesized using a low-cost and commercially available ligand *via* a rapid and scalable process that involves simple magnetic stirring in a water–formic acid mixture at 80 °C for 10–30 minutes. The activated **AL-MOF-1** can efficiently remove Pb^{2+} from aqueous solutions in both low (1 ppm) and high (84 ppm) concentrations in 10 min and 48 h, respectively, even in the presence of various competitive cations (Na^+, Mg^{2+}, Ca^{2+}, K^+). **AL-MOF-2** and **AL-MOF-3** are isolated through a post-synthetic, base-induced treatment of **AL-MOF-1** at room temperature, and they exhibit higher sorption capacities than the pristine material (233.0 and 254.0 mg Pb^{2+} per g, respectively) and exceptional selectivity towards Pb^{2+} even among various coexisting ions like Na^+, Mg^{2+}, Ca^{2+}, and K^+. Most importantly, the new Ce(IV)-MOFs in their composite forms with calcium alginate exhibited outstanding performance in column-based Pb^{2+} removal under continuous flow conditions. They can be regenerated and reused several times, demonstrating robustness and practical applicability for water decontamination. The excellent Pb^{2+} sorption properties of these materials under continuous flow conditions, involving several

uses of the MOF-based column with no loss of the sorption capacity, are unprecedented among MOF sorbents.

2.4 Characterization of the ion-loaded materials: mechanism of Pb^{2+} sorption

A detailed characterization of the ion-loaded materials was performed to investigate the sorption mechanism. As reported above, the zeta potential of the activated **AL-MOF-1** is negative, which favors electrostatic interactions between the MOF and Pb^{2+}. In addition, the free COOH groups of H_2BTCA^{2-} could facilitate the capture of Pb^{2+} by forming Pb^{2+}–COO^- bonds; however, this process appears to be slow, as indicated by the kinetics sorption studies. The PXRD of the Pb-loaded **AL-MOF-1** material shows a shift to higher 2-theta values than the activated and pristine materials. The PXRD pattern of Pb-loaded **AL-MOF-1** resembles that of **AL-MOF-2**, indicating a similar crystal structure (Fig. 6A). ^1H NMR data for (the digested) **AL-MOF-1** after Pb^{2+} sorption indicated a negligible amount of formate ligands, which justifies its similar PXRD pattern to that of **AL-MOF-2**, also containing an insignificant amount of formate ions (Fig. S39). This result revealed that the release of formate ligands, which are replaced by OH^-/H_2O terminal ligands, accompanies Pb^{2+} sorption by **AL-MOF-1**. SEM-EDS confirmed the presence of Pb^{2+} in the loaded material (Fig. S40). PXRD patterns for Pb-loaded **AL-MOF-2** and **AL-MOF-3** materials indicated that these compounds retain their structural characteristics upon Pb^{2+} sorption (Fig. 6A and Fig. S41). SEM-EDS confirmed the presence of Pb^{2+} in the loaded materials (Fig. S42 and S43). These materials contain no or negligible amounts of formate ligands, and thus, Pb^{2+} capture cannot affect their structural features, unlike the **AL-MOF-1** material.

Unfortunately, the IR spectra of the Pb^{2+}-loaded materials were not very informative, and no reliable conclusions could

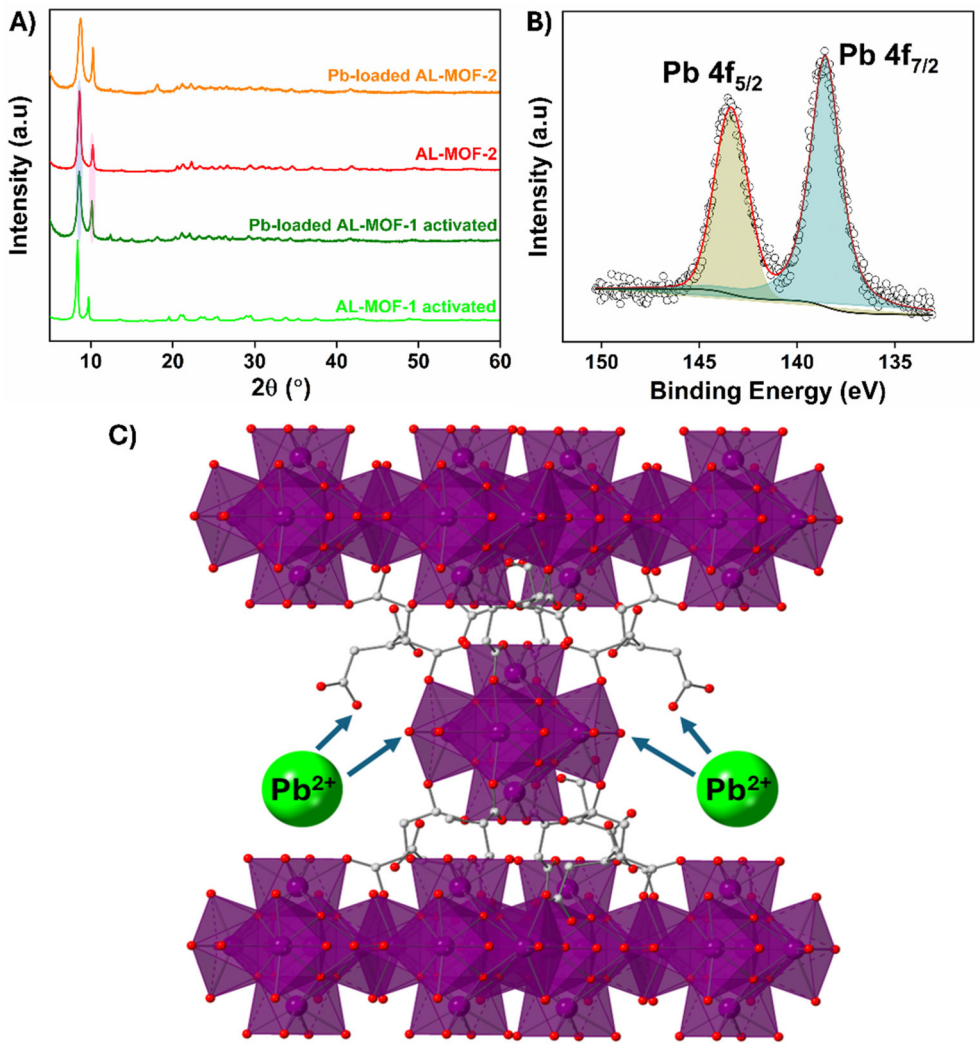

Fig. 6 (A) PXRD patterns of activated and Pb-loaded **AL-MOF-1** and **AL-MOF-2**; (B) XPS Pb 4f spectrum of Pb-loaded **AL-MOF-2**, showing the $4f_{5/2}$ and $4f_{7/2}$ core-level peaks at 143.4 and 138.6 eV, respectively; and (C) schematic representation of the Pb^{2+} sorption mechanism. In (B), the scatter points represent the experimental data, the red line corresponds to the fitting, the green line indicates the background, and the green and blue shaded areas represent the $4f_{5/2}$ and $4f_{7/2}$ core level signals, respectively.

be drawn regarding the sorption process (Fig. S44 and S45). To shed light on the Pb^{2+} sorption mechanism, XPS studies were carried out for the Pb-loaded **AL-MOF-2** (Fig. S46). The Pb-loaded **AL-MOF-1** and **3** were not studied, as they are isostructural with the Pb-containing **AL-MOF-2** (Fig. S47 and S48). The XPS results revealed the presence of Pb $4f_{5/2}$ and $4f_{7/2}$ peaks after Pb^{2+} capture (Fig. 6B). Importantly, the binding energy corresponding to the Pb $4f_{7/2}$ peak (138.6 eV) is very close to those of lead acetate and hydroxide compounds (138.6–138.7 eV) and notably lower than that of the $Pb(NO_3)_2$ precursor (139.3 eV), *i.e.*, the Pb^{2+} salt used in the sorption studies.[61,62] This result demonstrates a coordination environment for Pb^{2+} ions in Pb-loaded **AL-MOF-2** similar to that observed in lead acetate and hydroxide compounds. This strongly indicates the complexation of Pb^{2+} with the free carboxylate and terminal hydroxide ligands present in **AL-MOF-2**. Furthermore, there is a notable negative shift in the main component of the O 1s peak of the Pb-loaded **AL-MOF-2** (binding energy = 531.3 eV) compared to **AL-MOF-2** (binding energy = 531.9 eV) (Fig. S49). This can be explained by the deprotonation of free carboxylic acids in **AL-MOF-2** upon Pb^{2+} capture, with the resulting carboxylate O species exhibiting lower binding energy than the carboxylic oxygen atoms.[63] In addition, comparing the Ce : Na atomic ratios determined from EDS (Fig. S15, S19, S42 and S43), for **AL-MOF-2**, **3** (Ce : Na = 1 : 0.2 and 1 : 0.4 for **AL-MOF-2** and **3**, respectively) *versus* the corresponding values for the Pb-loaded materials (Ce : Na = 1 : 0.01 and 1 : 0.07 for Pb-loaded **AL-MOF-2** and **3**, respectively), it is evident that the Pb-loaded MOFs exhibit significantly smaller Na content compared to the pristine materials. This is presumably due to an ion-exchange process involving Pb^{2+} and Na^{+} cations. Besides carboxylate groups, terminal hydroxide groups can also bind Pb^{2+} ions, as revealed by the sorption results indicating enhanced sorption capacity of the MOF upon the replacement of formate ligands by terminal hydroxide/water groups (Fig. 6C). It should also be mentioned that the Pb^{2+} capture occurs on the surface of MOF particles as the diameter of the Pb^{2+} hydrated ion (~5.2 Å) is well above the pore sizes of the MOFs (1.9–4.7 Å for **AL-MOF-1** and even smaller pore sizes for **AL-MOF-2** and **AL-MOF-3**).

DFT studies focusing on Pb^{2+} sorption on hydroxide and carboxylate sites of defective UiO-66 structures, which are related to **AL-MOF-1**, **2**, and **3** materials, have been reported in the literature.[64] These indicate favorable interactions with both hydroxide and carboxylate groups. This finding aligns with the experimental results from the present work, indicating a significant contribution of both hydroxide and carboxylate functional groups to Pb^{2+} sorption.

3. Conclusions

In conclusion, three new Ce(IV) MOFs (**AL-MOF-1–3**) with the aliphatic polycarboxylic ligand H_4BTCA were described. **AL-MOF-1** was synthesized in high yield and on a large scale (up to 7.5 g) *via* a rapid (25–30 min) reaction in water–formic acid solution from low-cost and commercially available reagents at a modest temperature (80 °C), whereas **AL-MOF-2** and **3** were isolated *via* a room temperature treatment of **AL-MOF-1** with basic aqueous solutions. Although these materials are isolated as microcrystalline powders, their structure, connectivity, and general structural features can be elucidated *via* MicroED (for **AL-MOF-1** and **2**), revealing topological features not frequently observed in Ce(IV) MOFs. Specifically, these materials are based on 8-coordinated MOFs with four H_2BTCA^{2-} linkers per Ce_6 cluster and a **bcu** topology. Bridging formate and water-hydroxide terminal ligands complete the coordination sphere of Ce(IV) ions in **AL-MOF-1**. In contrast, in **AL-MOF-2** and **3**, the formate ligands were replaced by additional terminal water and hydroxide groups. Interestingly, treating **AL-MOF-2** and **3** with a formic acid solution restores **AL-MOF-1**. Considering that **AL-MOF-2** and **3** are non-porous materials (BET surface areas <10 $m^2\ g^{-1}$), the insertion of formic acid into their framework, resulting in the restoration of the **AL-MOF-1** material, indicates a breathing of their frameworks, which can be ascribed to the flexible aliphatic H_2BTCA^{2-} linkers. It is also interesting that bulkier carboxylic acids cannot alter the structure of these materials, revealing a specificity towards formic acid.

The three new MOFs, containing abundant free COOH and terminal OH ligands, were investigated for their Pb^{2+} sorption properties. **AL-MOF-1** could rapidly remove Pb^{2+} in low initial concentrations (1 ppm or less) from various aqueous media, including genuine water samples. However, its maximum sorption capacity was relatively low (58.0 ± 1.0 mg Pb per g). **AL-MOF-2** and **3**, with additional terminal hydroxide ligands replacing the formate groups and likely the presence of free deprotonated carboxylic groups, exhibited enhanced sorption capacities (233.0 and 254.0 mg Pb^{2+} per g) compared to **AL-MOF-1**. Importantly, all new MOFs in their composite forms with calcium alginate exhibited excellent capability for removing Pb^{2+} from aqueous media under continuous flow conditions, with high removal capacities, facile regeneration, and exceptional reusability. This performance for Pb^{2+} sorption under flow exceeds that of other MOF-based sorbents, making the new MOFs attractive for practical applications in water treatment. Experimental data demonstrate that the remarkable sorption properties of the materials are due to the strong interactions of Pb^{2+} with the free carboxylate groups and terminal hydroxide ligands. Overall, the present work emphasizes the potential of MOFs based on aliphatic polycarboxylate linkers for water remediation applications, as these materials combine low cost, straightforward aqueous-based synthesis, and multiple functional groups that strongly bind various toxic species. Further work for developing this category of promising sorbents is underway in our laboratory.

Author contributions

N. E. Anastasiadis and V. I. Karagianni: investigation, formal analysis, and writing – original draft. P. Kotidis: investigation and formal analysis. C. Dimitriou: investigation and formal

analysis. I. Vamvasakis: investigation and formal analysis. T. Lazarides: investigation, formal analysis, writing – review & editing, and resources. G. S. Papaefstathiou: investigation, formal analysis, writing – review & editing, and resources. Y. Deligiannakis: investigation, formal analysis, writing – review & editing, and resources. G. S. Armatas: investigation, formal analysis, writing – review & editing, and resources. M. J. Manos: conceptualization, supervision, resources, and writing – original draft.

Conflicts of interest

There are no conflicts to declare.

Data availability

The data supporting this article are provided within the manuscript and the SI: additional experimental details, materials and methods, PXRD patterns, Le Bail and Rietveld plots, TGA, BET and zeta-potential diagrams, FE-SEM images, ^{1}H-NMR, XPS, IR and EDS spectra, kinetics, column sorption data, and tables with comparisons of Pb^{2+} sorbents. See DOI: **https://doi.org/10.1039/d5qi01181g**.

CCDC 2451530–2451532 and 2473842 contain the supplementary crystallographic data for this paper.[65a–d]

Acknowledgements

This research has been co-financed by the European Union NextGenerationEU under the call RESEARCH – CREATE – INNOVATE 16971 Recovery and Resilience Facility (project code: TAEDK-06193). We also acknowledge the NMR Centre of the Network of Research Supporting Laboratories and the Microscopy Unit of the Chemistry Department at the University of Ioannina for providing facility access.

References

1 A. Schneemann, V. Bon, I. Schwedler, I. Senkovska, S. Kaskel and R. A. Fischer, Flexible metal-organic frameworks, *Chem. Soc. Rev.*, 2014, **43**, 6062–6096.
2 D. Alezi, Y. Belmabkhout, M. Suyetin, P. M. Bhatt, L. J. Weseliński, V. Solovyeva, K. Adil, I. Spanopoulos, P. N. Trikalitis, A. H. Emwas and M. Eddaoudi, MOF Crystal Chemistry Paving the Way to Gas Storage Needs: Aluminum-Based soc -MOF for CH_4, O_2, and CO_2 Storage, *J. Am. Chem. Soc.*, 2015, **137**, 13308–13318.
3 M. J. Rosseinsky, Recent developments in metal-organic framework chemistry: Design, discovery, permanent porosity and flexibility, *Microporous Mesoporous Mater.*, 2004, **73**, 15–30.
4 Z. Chen, K. Ma, J. J. Mahle, H. Wang, Z. H. Syed, A. Atilgan, Y. Chen, J. H. Xin, T. Islamoglu, G. W. Peterson and O. K. Farha, Integration of Metal-Organic Frameworks on Protective Layers for Destruction of Nerve Agents under Relevant Conditions, *J. Am. Chem. Soc.*, 2019, **141**, 20016–20021.
5 G. Maurin, C. Serre, A. Cooper and G. Férey, The new age of MOFs and of their porous-related solids, *Chem. Soc. Rev.*, 2017, **46**, 3104–3107.
6 S. Kitagawa, R. Kitaura and S. I. Noro, Functional porous coordination polymers, *Angew. Chem., Int. Ed.*, 2004, **43**, 2334–2375.
7 M. Eddaoudi, H. Li and O. M. Yaghi, Highly porous and stable metal-organic frameworks: Structure design and sorption properties, *J. Am. Chem. Soc.*, 2000, **122**, 1391–1397.
8 P. Kumar, A. Pournara, K. H. Kim, V. Bansal, S. Rapti and M. J. Manos, Metal-organic frameworks: Challenges and opportunities for ion-exchange/sorption applications, *Prog. Mater. Sci.*, 2017, **86**, 401–479.
9 C. Xiao, A. Khayambashi and S. Wang, Separation and Remediation of $99TcO_4^-$ from Aqueous Solutions, *Chem. Mater.*, 2019, **31**, 6786–6795.
10 J. Li, X. Wang, G. Zhao, C. Chen, Z. Chai, A. Alsaedi, T. Hayat and X. Wang, Metal-organic framework-based materials: Superior adsorbents for the capture of toxic and radioactive metal ions, *Chem. Soc. Rev.*, 2018, **47**, 2322–2356.
11 S. Dutta, Y. D. More, S. Fajal, W. Mandal, G. K. Dam and S. K. Ghosh, Ionic metal-organic frameworks (iMOFs): progress and prospects as ionic functional materials, *Chem. Commun.*, 2022, **58**, 8855–8871.
12 P. Deria, W. Bury, J. T. Hupp and O. K. Farha, Versatile functionalization of the nu-1000 platform by solvent-assisted ligand incorporation, *Chem. Commun.*, 2014, **50**, 1965–1968.
13 A. D. Pournara, S. Rapti, A. Valmas, I. Margiolaki, E. Andreou, G. S. Armatas, A. C. Tsipis, J. C. Plakatouras, D. L. Giokas and M. J. Manos, Alkylamino-terephthalate ligands stabilize 8-connected Zr^{4+} MOFs with highly efficient sorption for toxic Se species, *J. Mater. Chem. A*, 2021, **9**, 3379–3387.
14 D. Evangelou, A. Pournara, C. Tziasiou, E. Andreou, G. S. Armatas and M. J. Manos, Robust Al^{3+} MOF with Selective As(V) Sorption and Efficient Luminescence Sensing Properties toward Cr(VI), *Inorg. Chem.*, 2022, **61**, 2361–2370.
15 Z. Hu, Y. Peng, Z. Kang, Y. Qian and D. Zhao, A Modulated Hydrothermal (MHT) Approach for the Facile Synthesis of UiO-66-Type MOFs, *Inorg. Chem.*, 2015, **54**, 4862–4868.
16 S. Rapti, A. Pournara, D. Sarma, I. T. Papadas, G. S. Armatas, Y. S. Hassan, M. H. Alkordi, M. G. Kanatzidis and M. J. Manos, Rapid, green and inexpensive synthesis of high quality UiO-66 amino-functionalized materials with exceptional capability for removal of hexavalent chromium from industrial waste, *Inorg. Chem. Front.*, 2016, **3**, 635–644.
17 S. Wang, M. Wahiduzzaman, L. Davis, A. Tissot, W. Shepard, J. Marrot, C. Martineau-Corcos, D. Hamdane, G. Maurin, S. Devautour-Vinot and C. Serre, A robust zirco-

nium amino acid metal-organic framework for proton conduction, *Nat. Commun.*, 2018, **9**, 1660.

18 K. E. Diab, E. Salama, H. S. Hassan, A. A. El-Moneim and M. F. Elkady, Bio-zirconium metal–organic framework regenerable bio-beads for the effective removal of organophosphates from polluted water, *Polymers*, 2021, **13**, 3869.

19 P. Liu, P. Yang, J. Yang and J. Gu, One-pot synthesis of sulfonic acid functionalized Zr-MOFs for rapid and specific removal of radioactive Ba^{2+}, *Chem. Commun.*, 2021, **57**, 5534–5537.

20 P. Yang, Y. Shu, Q. Zhuang, Y. Li and J. Gu, A robust MOF-based trap with high-density active alkyl thiol for the super-efficient capture of mercury, *Chem. Commun.*, 2019, **55**, 12972–12975.

21 X. Gao, B. Liu and X. Zhao, Thiol-decorated defective metal-organic framework for effective removal of mercury (II) ion, *Chemosphere*, 2023, **317**, 137891.

22 C. Tziasiou, A. D. Pournara, M. J. Manos and D. L. Giokas, Dispersive solid phase extraction of noble metal nanoparticles from environmental samples on a thiol-functionalized Zirconium(IV) metal organic framework and determination with atomic absorption spectrometry, *Microchem. J.*, 2023, **195**, 109387.

23 C. Tziasiou, E. K. Andreou, G. S. Armatas, M. J. Manos, A. D. Pournara and D. L. Giokas, Zr^{4+}-mercaptosuccinate MOF for the uptake and recovery of gold nanoparticles and gold ions under batch and continuous flow conditions, *Chem. Eng. J.*, 2024, **487**, 151107.

24 Y. F. Zhang, Q. Wang, D. X. Xue and J. Bai, Single-Crystal Synthesis and Diverse Topologies of Hexanuclear CeIV-Based Metal-Organic Frameworks, *Inorg. Chem.*, 2020, **59**(16), 11233–11237.

25 R. D'Amato, A. Donnadio, M. Carta, C. Sangregorio, D. Tiana, R. Vivani, M. Taddei and F. Costantino, Water-Based Synthesis and Enhanced CO_2 Capture Performance of Perfluorinated Cerium-Based Metal-Organic Frameworks with UiO-66 and MIL-140 Topology, *ACS Sustainable Chem. Eng.*, 2019, **7**(1), 394–402.

26 M. Lammert, M. T. Wharmby, S. Smolders, B. Bueken, A. Lieb, K. A. Lomachenko, D. D. Vos and N. Stock, Cerium-based metal organic frameworks with UiO-66 architecture: Synthesis, properties and redox catalytic activity, *Chem. Commun.*, 2015, **51**, 12578–12581.

27 J. Jacobsen, B. Achenbach, H. Reinsch, S. Smolders, F. D. Lange, G. Friedrichs, D. D. Vos and N. Stock, The first water-based synthesis of Ce(IV)-MOFs with saturated chiral and achiral C4-dicarboxylate linkers, *Dalton Trans.*, 2019, **48**, 8433–8441.

28 F. Li, C. Duan, H. Zhang, X. Yan, J. Li and H. Xi, Hierarchically Porous Metal-Organic Frameworks: Green Synthesis and High Space-Time Yield, *Ind. Eng. Chem. Res.*, 2018, **57**(28), 9136–9143.

29 M. Rubio-Martinez, C. Avci-Camur, A. W. Thornton, I. Imaz, D. Maspoch and M. R. Hill, New synthetic routes towards MOF production at scale, *Chem. Soc. Rev.*, 2017, **46**, 3453–3480.

30 J. Ren, X. Dyosiba, N. M. Musyoka, H. W. Langmi, M. Mathe and S. Liao, Review on the current practices and efforts towards pilot-scale production of metal-organic frameworks (MOFs), *Coord. Chem. Rev.*, 2017, **352**, 187–219.

31 S. E. Henkelis, D. J. Vogel, P. C. Metz, N. R. Valdez, M. A. Rodriguez, D. X. Rademacher, S. Purdy, S. J. Percival, J. M. Rimsza, K. Page and T. M. Nenoff, Kinetically Controlled Linker Binding in Rare Earth-2,5-Dihydroxyterepthalic Acid Metal-Organic Frameworks and Its Predicted Effects on Acid Gas Adsorption, *ACS Appl. Mater. Interfaces*, 2021, **13**(47), 56337–56347.

32 T. J. M. M. Ntep, H. Reinsch, J. Liang and C. Janiak, Acetylenedicarboxylate-based cerium(IV) metal-organic framework with fcu topology: A potential material for air cleaning from toxic halogen vapors, *Dalton Trans.*, 2019, **48**, 15849–15855.

33 M. Lammert, C. Glißmann, H. Reinsch and N. Stock, Synthesis and Characterization of New Ce(IV)-MOFs Exhibiting Various Framework Topologies, *Cryst. Growth Des.*, 2017, **17**(3), 1125–1131.

34 M. Cavallo, C. Atzori, M. Signorile, F. Costantino, D. M. Venturi, A. Koutsianos, K. A. Lomachenko, L. Calucci, F. Martini, A. Giovanelli, M. Geppi, V. Crocellà and M. Taddei, Cooperative CO_2 adsorption mechanism in a perfluorinated Ce(IV)-based metal organic framework, *J. Mater. Chem. A*, 2023, **11**, 5568–5583.

35 X. Q. Wang, J. Yang, M. Zhang, D. Wu, T. Hu and J. Yang, Highly stable lanthanide(iii) metal-organic frameworks as ratiometric fluorescence sensors for vitamin B6, *Dalton Trans.*, 2023, **52**, 13387–13394.

36 M. Lammert, H. Reinsch, C. A. Murray, M. T. Wharmby, H. Terraschke and N. Stock, Synthesis and structure of Zr (IV)- and Ce(IV)-based CAU-24 with 1,2,4,5-tetrakis(4-carboxyphenyl)benzene, *Dalton Trans.*, 2016, **45**, 18822–18826.

37 S. Smolders, A. Struyf, H. Reinsch, B. Bueken, T. Rhauderwiek, L. Mintrop, P. Kurz, N. Stock and D. E. De Vos, A precursor method for the synthesis of new Ce(IV) MOFs with reactive tetracarboxylate linkers, *Chem. Commun.*, 2018, **54**, 876–879.

38 A. A. Coelho, TOPAS and TOPAS-Academic: an optimization program integrating computer algebra and crystallographic objects written in C++, *J. Appl. Crystallogr.*, 2018, **51**, 210–218.

39 C. F. MacRae, I. Sovago, S. J. Cottrell, P. T. A. Galek, P. McCabe, E. Pidcock, M. Platings, G. P. Shields, J. S. Stevens, M. Towler and P. A. Wood, Mercury 4.0: From visualization to analysis, design and prediction, *J. Appl. Crystallogr.*, 2020, **53**, 226–235.

40 R. C. Klet, Y. Liu, T. C. Wang, J. T. Hupp and O. K. Farha, Evaluation of Brønsted acidity and proton topology in Zr- and Hf-based metal-organic frameworks using potentiometric acid-base titration, *J. Mater. Chem. A*, 2016, **4**, 1479–1485.

41 D. J. Morgan, Photoelectron spectroscopy of ceria: Reduction, quantification and the myth of the vacancy peak in XPS analysis, *Surf. Interface Anal.*, 2023, **55**(11), 845–850.

42 D. M. Venturi, M. S. Notari, L. Trovarelli, E. Mosconi, A. A. Alothman, A. Molokova, N. Ruser, C. Meier, B. Achenbach, K. A. Lomachenko, T. del Giacco, F. Costantino and N. Stock, Synthesis, Structure and (Photo)Catalytic Behavior of Ce-MOFs Containing Perfluoroalkylcarboxylate Linkers: Experimental and Theoretical Insights, *Chem. – Eur. J.*, 2024, **30**, e202400433.

43 Q. Peng, J. Guo, Q. Zhang, J. Xiang, B. Liu, A. Zhou, R. Liu and Y. Tian, Unique lead adsorption behavior of activated hydroxyl group in two-dimensional titanium carbide, *J. Am. Chem. Soc.*, 2014, **136**(11), 4113–4116.

44 X. Zhao, G. Zhang, Q. Jia, C. Zhao, W. Zhou and W. Li, Adsorption of Cu(II), Pb(II), Co(II), Ni(II), and Cd(II) from aqueous solution by poly(aryl ether ketone) containing pendant carboxyl groups (PEK-L): Equilibrium, kinetics, and thermodynamics, *Chem. Eng. J.*, 2011, **171**(1), 152–158.

45 J. Yang, X. Li, Z. Xiong, M. Wang and Q. Liu, Environmental pollution effect analysis of lead compounds in China based on life cycle, *Int. J. Environ. Res. Public Health*, 2020, **17**(7), 2184.

46 K. Raj and A. P. Das, Lead pollution: Impact on environment and human health and approach for a sustainable solution, *J. Environ. Chem. Ecotoxicol.*, 2023, **5**, 79–85.

47 V. Kumar, S. K. Dwivedi and S. Oh, A critical review on lead removal from industrial wastewater: Recent advances and future outlook, *J. Water Process Eng.*, 2022, **45**, 102518.

48 M. J. Manos and M. G. Kanatzidis, Sequestration of heavy metals from water with layered metal sulfides, *Chem. – Eur. J.*, 2009, **15**, 4779–4784.

49 A. D. Pournara, D. A. Evangelou, C. Roukounaki, E. K. Andreou, G. S. Armatas, T. Lazarides and M. J. Manos, Highly efficient sorption and luminescence sensing of oxoanionic species by 8-connected alkyl-amino functionalized Zr^{4+} MOFs, *Dalton Trans.*, 2022, **51**, 17301–17309.

50 A. D. Pournara, S. Rizogianni, D. A. Evangelou, E. K. Andreou, G. S. Armatas and M. J. Manos, Zr^{4+}-terephthalate MOFs with 6-connected structures, highly efficient As(iii/v) sorption and superhydrophobic properties, *Chem. Commun.*, 2022, **58**, 8862–8865.

51 S. Rapti, A. Pournara, D. Sarma, I. T. Papadas, G. S. Armatas, A. C. Tsipis, T. Lazarides, M. G. Kanatzidis and M. J. Manos, Selective capture of hexavalent chromium from an anion-exchange column of metal organic resin-alginic acid composite, *Chem. Sci.*, 2016, **7**, 2427–2436.

52 S. Rapti, D. Sarma, S. A. Diamantis, E. Skliri, G. S. Armatas, A. C. Tsipis, Y. S. Hassan, M. Alkordi, C. D. Malliakas, M. G. Kanatzidis, T. Lazarides, J. C. Plakatouras and M. J. Manos, All in one porous material: Exceptional sorption and selective sensing of hexavalent chromium by using a Zr^{4+} MOF, *J. Mater. Chem. A*, 2017, **5**, 14707–14719.

53 A. D. Pournara, A. Margariti, G. D. Tarlas, A. Kourtelaris, V. Petkov, C. Kokkinos, A. Economou, G. S. Papaefstathiou and M. J. Manos, A Ca^{2+} MOF combining highly efficient sorption and capability for voltammetric determination of heavy metal ions in aqueous media, *J. Mater. Chem. A*, 2019, **7**, 15432–15443.

54 J. Lou, Q. Fu, L. Yu, H. Yuan, J. Zhao, L. Wang, D. Shi, C. Mo and J. Luo, Highly effective removal of Pb^{2+} from wastewater by nickel-based metal organic framework, *J. Solid State Chem.*, 2022, **315**, 123535.

55 A. D. Pournara, C. G. Bika, X. Chen, T. Lazarides, S. Kaziannis, P. Feng and M. J. Manos, A bifunctional robust metal sulfide with highly selective capture of Pb^{2+} ions and luminescence sensing ability for heavy metals in aqueous media, *Inorg. Chem. Front.*, 2021, **8**, 4052–4061.

56 A. D. Pournara, S. Rapti, T. Lazarides and M. J. Manos, A dithiocarbamate-functionalized Zr^{4+} MOF with exceptional capability for sorption of Pb^{2+} in aqueous media, *J. Environ. Chem. Eng.*, 2021, **9**(4), 105474.

57 R. Ricco, K. Konstas, M. J. Styles, J. J. Richardson, R. Babarao, K. Suzuki, P. Scopece and P. Falcaro, Lead(II) uptake by aluminium based magnetic framework composites (MFCs) in water, *J. Mater. Chem. A*, 2015, **3**, 19822–19831.

58 R. Li, H. Deng, X. Zhang, J. J. Wang, M. K. Awasthi, Q. Wang, R. Xiao, B. Zhou, J. Du and Z. Zhang, High-efficiency removal of Pb(II) and humate by a CeO_2–MoS_2 hybrid magnetic biochar, *Bioresour. Technol.*, 2019, **273**, 335–340.

59 H. Zhu, J. Yuan, X. Tan, W. Zhang, M. Fang and X. Wang, Efficient removal of Pb^{2+} by Tb-MOFs: identifying the adsorption mechanism through experimental and theoretical investigations, *Environ. Sci.: Nano*, 2019, **6**, 261–272.

60 Q. Fu, J. Lou, L. Peng, R. Zhang, S. Zhou, P. Wu, W. Yan, C. Mo and J. Luo, Iron based metal organic framework for efficient removal of Pb^{2+} from wastewater, *J. Solid State Chem.*, 2021, **300**, 122188.

61 P. A. Bertrand and P. D. Fleischauer, X-ray photoelectron spectroscopy study of the surface adsorption of lead naphthenate, *J. Vac. Sci. Technol.*, 1980, **17**, 1309–1314.

62 V. I. Nefedov, Y. V. Salyn, P. M. Solozhenkin and G. Y. Pulatov, X-ray photoelectron study of surface compounds formed during flotation of minerals, *Surf. Interface Anal.*, 1980, **2**(5), 170–172.

63 B. Lindberg, A. Berndtsson, R. Nilsson, R. Nyholm, O. Exner, L. Fernholt, G. Gundersen, C. J. Nielsen, B. N. Cyvin and S. J. Cyvin, An ESCA Investigation of Ambident Ions and Tautomerism. N-Cyanobenzamides and Benzohydroxamic Acids, *Acta Chem. Scand.*, 1978, **32A**, 353–359.

64 C. S. Cox, V. C. Galicia and M. Lessio, Computational Investigation of Adsorptive Removal of Pb^{2+} from Water by the UiO-66 Metal–Organic Framework: Comparison of Adsorption Sites on Defects and Functionalised Linkers, *Aust. J. Chem.*, 2022, **75**, 142–154.

65 (*a*) N. E. Anastasiadis, V. I. Karagianni, P. Kotidis, C. Dimitriou, I. Vamvasakis, T. Lazarides, G. S. Papaefstathiou, Y. Deligiannakis, G. S. Armatas, E. Buchsteiner and M. J. Manos, CCDC 2451530: Experimental Crystal Structure Determination, 2025, DOI: **10.5517/ccdc.csd.cc2n90mm**; (*b*) N. E. Anastasiadis, V. I. Karagianni, P. Kotidis, C. Dimitriou, I. Vamvasakis,

T. Lazarides, G. S. Papaefstathiou, Y. Deligiannakis, G. S. Armatas, E. Buchsteiner and M. J. Manos, CCDC 2451531: Experimental Crystal Structure Determination, 2025, DOI: 10.5517/ccdc.csd.cc2n90nn; (*c*) N. E. Anastasiadis, V. I. Karagianni, P. Kotidis, C. Dimitriou, I. Vamvasakis, T. Lazarides, G. S. Papaefstathiou, Y. Deligiannakis, G. S. Armatas, E. Buchsteiner and M. J. Manos, CCDC 2451532: Experimental Crystal Structure Determination, 2025, DOI: 10.5517/ccdc.csd.cc2n90pp; (*d*) N. E. Anastasiadis, V. I. Karagianni, P. Kotidis, C. Dimitriou, I. Vamvasakis, T. Lazarides, G. S. Papaefstathiou, Y. Deligiannakis, G. S. Armatas, E. Buchsteiner and M. J. Manos, CCDC 2473842: Experimental Crystal Structure Determination, 2025, DOI: 10.5517/ccdc.csd.cc2p17cc.